Continental Shelf Research 104 (2015) 1–14

Contents lists available at ScienceDirect

Continental Shelf Research

journal homepage: www.elsevier.com/locate/csr

Characteristics of storms driving wave-induced seafloor mobility on the U.S. East Coast continental shelf

P. Soupy Dalyander [a,*], Bradford Butman [b]

[a] U.S. Geological Survey, 600 4th Street S., St. Petersburg, FL 33701, USA
[b] U.S. Geological Survey, 384 Woods Hole Road, Woods Hole, MA 02543, USA

ARTICLE INFO

Article history:
Received 18 August 2014
Received in revised form
23 April 2015
Accepted 9 May 2015
Available online 13 May 2015

Keywords:
Bottom wave stress
Seafloor mobility
Extratropical storms
Tropical storms
U.S. East Coast continental shelf

ABSTRACT

This study investigates the relationship between spatial and temporal patterns of wave-driven sediment mobility events on the U.S. East Coast continental shelf and the characteristics of the storms responsible for them. Mobility events, defined as seafloor wave stress exceedance of the critical stress of 0.35 mm diameter sand (0.2160 Pa) for 12 or more hours, were identified from surface wave observations at National Data Buoy Center buoys in the Middle Atlantic Bight (MAB) and South Atlantic Bight (SAB) over the period of 1997–2007. In water depths ranging from 36–48 m, there were 4–9 mobility events/year of 1–2 days duration. Integrated wave stress during events (IWAVES) was used as a combined metric of wave-driven mobility intensity and duration. In the MAB, over 67% of IWAVES was caused by extra-tropical storms, while in the SAB, greater than 66% of IWAVES was caused by tropical storms. On average, mobility events were caused by waves generated by storms located 800+ km away. Far-field hurricanes generated swell 2–4 days before the waves caused mobility on the shelf. Throughout most of the SAB, mobility events were driven by storms to the south, east, and west. In the MAB and near Cape Hatteras, winds from more northerly storms and low-pressure extratropical systems in the mid-western U.S. also drove mobility events. Waves generated by storms off the SAB generated mobility events along the entire U.S. East Coast shelf north to Cape Cod, while Cape Hatteras shielded the SAB area from swell originating to the north offshore of the MAB.

Published by Elsevier Ltd.

1. Introduction

Near-bottom currents driven by tides, winds, and large-scale patterns in ocean circulation combine with wave orbital motion to induce a shear stress at the seafloor, with the largest stress events typically associated with storms (Dalyander et al., 2013; Grant and Madsen, 1979; Madsen, 1994; Nielsen, 1992; Oberle et al., 2014; Soulsby, 1997). When the bottom stress acting on the seafloor (i.e., the skin friction) exceeds a grain size and density specific critical threshold, sediment begins to move. Wave-driven bottom stress is larger for longer period waves; for example, in 50-m water depth, a JONSWAP (Hasselmann et al., 1973) spectrum of waves with significant wave height of 5-m and dominant wave period of 8, 10, and 14 s causes a stress on 0.35 mm diameter grains of 0.091, 0.293, and 0.747 Pa, respectively (Butman et al., 2008; Madsen, 1994; Wiberg and Sherwood, 2008). Through this interaction with the bottom (including the movement of sediment), long period waves dissipate energy during propagation over the shelf (e.g., Ardhuin et al., 2002, 2003; Herbers et al., 2012). As a result, more energetic shorter period swell or wind waves may dominate shear stress over portions of the inner- to mid-shelf. Although the physics of wave-driven bottom stress are generally well-known, the origins of the waves that cause the largest bottom stress and sediment mobility events have not been investigated. Understanding these relationships provides insight into processes currently shaping the shelf sedimentary environment and develops a framework for assessing the effects of the future wave-stress environment.

Investigations of the relationship between synoptic weather systems and seafloor mobility have primarily focused on km-scale geographic areas (e.g., Austin and Lentz, 1999; Kim et al., 1997; Warner et al., 2012). Warner et al. (2012) explored how storms impact waves and circulation at a 10 m site offshore of South Carolina (SC; Fig. 1) using the Austin and Lentz (1999) classification system for U.S. East Coast storms. This system divides wind events into those where the low pressure system passes to the east, but the site is still within the wind field of the system; those where the storm tracks north of the region from west to east and a cold front passes over the Cape Hatteras area; and those where the storm tracks west of the region from south to north and a warm

* Corresponding author. Fax +1 727 502 8001.
E-mail address: sdalyander@usgs.gov (P.S. Dalyander).

http://dx.doi.org/10.1016/j.csr.2015.05.003
0278-4343/Published by Elsevier Ltd.

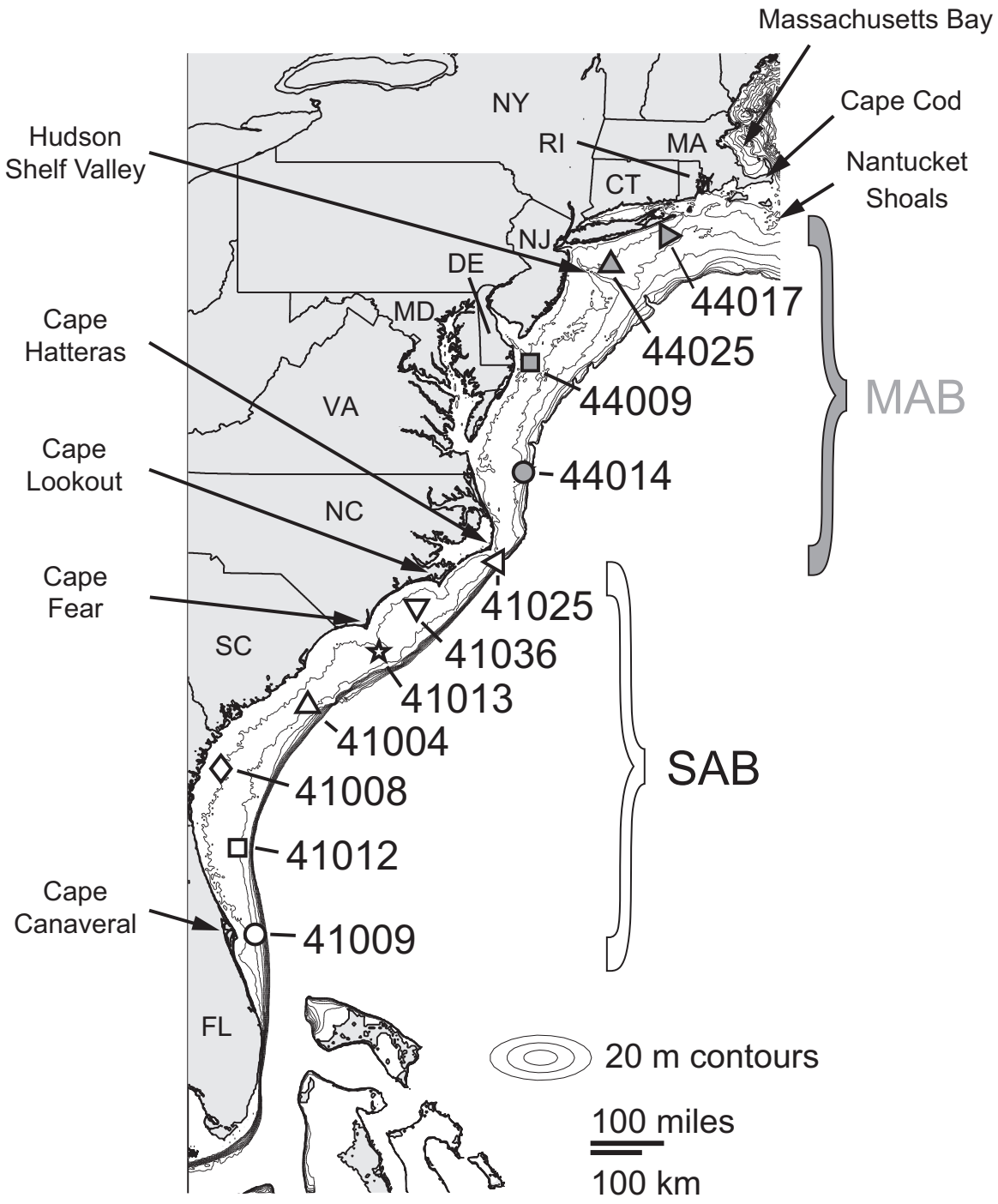

Fig. 1. Map showing the location of buoys from which surface wave data were obtained in the Middle Atlantic Bight (MAB; gray symbols) and the South Atlantic Bight (SAB; white symbols). Symbol shapes delineating individual buoys are the same as used in Figs. 7 and 9. State abbreviations are Florida (FL), North Carolina (NC), South Carolina (SC), Virginia (VA), Maryland (MD), Delaware (DE), New Jersey (NJ), New York (NY), Connecticut (CT), Rhode Island (RI), and Massachusetts (MA).

front passes the area. Warner et al. (2012) found that inshore low-pressure centers could drive significant events at their ~10 m site. Kim et al. (1997) characterized phases of inner shelf sediment response to a passing near-field extratropical storm. Studies along the Pacific Coast of the United States (Drake and Cacchione, 1985; Sherwood et al., 1994), the Gulf of Mexico (Snedden et al., 1988), the Mediterranean Sea (Dufois et al., 2008), and Australia (Gagan et al., 1990) have similarly identified sediment suspension at selected locations on the inner shelf in response to near- and far-field storms. Swell from the Pacific Ocean was identified through a numerical modeling study as driving sediment suspension along a broad region of the shelf along the coast of Australia (Porter-Smith et al., 2004), but the relationship between storm characteristics and shelf response was not explored.

Studies characterizing storms have focused on the atmosphere, sea surface, or onshore, classifying events based on origin and track and benchmarking them by wind speed, central pressure, wave height, or coastal damage (e.g., Davis et al., 1993; Dolan and Davis, 1992; Hart and Grumm, 2001; Keim et al., 2004; Mather et al., 1964; Simpson, 1974; Zielinski, 2002). For example, Davis et al. (1993) considered storms impacting Cape Hatteras and found that "Bahamas lows" and "Florida lows", two types of storms

which originate to the south/southeast of Florida and slowly move north, are the strongest of the extratropical storms when assessed by wave height and wave power, a measure including both total wave energy and storm duration.

Butman et al. (2008) developed a metric for wave-induced bottom stress at a site in Massachusetts Bay (Fig. 1). Surface wave observations of significant wave height and peak wave period were used to estimate bottom wave stress. Integrated Wave Stress (IWAVES), calculated as the sum of stress over 0.1 Pa, was used to rank storm events. The ranking was applied at a single site and identified extratropical Nor'Easters as the storm type responsible for large bottom stress events. The current study uses a modified IWAVES metric to quantify storms causing seafloor mobility.

The goals of the present study are to (1) identify the source of waves that drive seafloor mobility events on the U.S. East Coast continental shelf; (2) determine the relationship between storm characteristics and resultant seafloor mobility; and (3) investigate the spatial and temporal variability of mobility.

2. Study site characteristics

The U.S. East Coast can be divided into two regions: the Middle Atlantic Bight (MAB), extending from Cape Cod south to Cape Hatteras, and the South Atlantic Bight (SAB), extending from Cape Hatteras to the southern terminus of Florida (Fig. 1). The continental shelf is widest in the northern MAB (~100 km) and mid-SAB (~130 km), narrowing offshore of Cape Hatteras (~40 km) and in the southern SAB (~20 km). Sediment texture varies, generally consisting of medium/coarse to fine sand closer to the coast and fining to a mixture of silt and clay at the shelf break (McMullen et al., 2011). An anomaly is the "Mud Patch", a 100 km alongshore and 50 km cross-shelf deposit south of Cape Cod (Fig. 1) of greater than 25% mud in water depths of 55–65 m (Reid et al., 2005; Twichell et al., 1981). In the MAB, the bulk of surface sediments away from shore are Holocene quartz deposits, with an increasing percentage of carbonate moving south toward Florida (Ginsburg and James, 1974). The shelf has a shallow slope ranging from 0.4 to 1 m/km (Ginsburg and James, 1974).

The U.S. East Coast is subject to tropical storms and hurricanes during the summer months (TS) and extratropical storms (ETS; also known as Nor'Easters) predominantly from October to March (Zhang et al., 2000). The frequency of TS making landfall is highest in the SAB (Fig. 1), where the average return interval along any 80 km stretch of coast is ~40 years. The landfall frequency decreases northward to a return interval of more than 80 years, with the largest drop north of Virginia (Fig. 1; McAdie et al., 2009; Simpson and Riehl, 1981). In contrast, multiple ETS occur each year and are the dominant cause of episodic storm erosion along the shoreline of the U.S. East Coast (Zhang et al., 2001).

TS are low pressure systems that form over the ocean and derive energy from a central warm core (McAdie et al., 2009). These storms have a strong pressure gradient (on average 20 mb/100 km), resulting in powerful winds (up to 252 km/h or higher) generally confined near the center of the storm (Dolan and Davis, 1992; McAdie et al., 2009). Hurricanes typically impact ~150 km of coastline (Zhang et al., 2001). In contrast, ETS derive their strength from a horizontal temperature gradient originating out from a cold core (McAdie et al., 2009). The gradient in pressure across ETS is on average 5 mb/100 km, resulting in winds ranging from 20 to 30 km/h and extending over a large spatial area. Some ETS last for days and impact the entire U.S. East Coast (Dolan and Davis, 1992; Zhang et al., 2001).

Both TS and ETS drive sediment mobility on the U.S. East Coast continental shelf (Butman et al., 1979; Chang et al., 2001; Churchill et al., 1994; Lyne et al., 1990a; Twichell et al., 1981). In the MAB, waves dominate bottom shear stress at depths of 20–100 m throughout most of the region, with a modest contribution during storms from wind-driven currents (Dalyander et al., 2013). Lyne et al. (1990a; 1990b) determined that critical stress exceedance and resuspension in the MAB in depths of 60–80 m only occurred during storms. Harris and Coleman (1998) found that on the U.S. East Coast, swell waves induced mobility of 0.1 mm sand on the inner- to mid-shelf for 1–50% of a one year period in 1994–1995.

3. Methods

3.1. Identifying seafloor mobility events from buoy observations

Wave data were obtained from two National Oceanic and Atmospheric Administration (NOAA) National Data Buoy Center (NDBC) buoys in the MAB (44025 and 44014) and two in the SAB (41004 and 41009) (Fig. 1, Table 1). Annual analysis of the wave data was conducted with years starting on March 1 to keep consecutive winter months in the same year. Only years with $>75\%$ data coverage were analyzed. These sites were selected because they are within the mid-shelf water depth range of interest. In addition, they have nearly continuous data availability for March 1997 to March 2007 (cumulative data coverage of 9.4, 8.7, 9.3, and 9.7 years for buoys 44025, 44014, 41004, and 41009, respectively), the ten-year period covered by an ETS database used to identify the origin of storm waves. There were some data gaps, the largest being 111 days in winter of 1999 at buoy 44025 and 165 days in winter of 1997 at buoy 44014.

Data from NDBC buoys are typically provided hourly; higher frequency (20 min interval) data were interpolated to hourly intervals for consistency. Bottom orbital velocity (u_{br}) and representative period (T_{br}) were calculated from surface wave parameters by assuming a JONSWAP (Hasselmann et al., 1973) spectral shape and following the parameterized approach of Wiberg and Sherwood (2008). Values calculated using the parameterized spectrum and compared to those from the full spectrum at the sites used in this study were also found to be skillful for u_{br} (RMSE of 0.02 m/s) and T_{br} (RMSE of 1.56 s). The parameterized spectrum allowed use of data collected prior to deployment of buoys that resolve the full wave spectrum.

Derived values of u_{br} and T_{br} were used to calculate the wave bottom stress acting on the seafloor following Madsen (1994). The relevant stress component for seafloor mobility is the 'effective stress' or skin friction (τ_w), the force acting on sand grains, calculated using sediment diameter as the roughness in stress calculations (Nielsen, 1992; Soulsby, 1997). The average (mean) median grain size (D_{50}) of non-cohesive sediments based on 307 samples distributed throughout the MAB and SAB in 30–50 m is 0.27 mm with a standard deviation ($\pm 1\sigma$) of 0.18 mm (calculated from data within McMullen et al., 2011). Seafloor mobility varies

Table 1
Table of sites in the Middle Atlantic Bight (MAB) and South Atlantic Bight (SAB) used in mobility and storm wave origin analysis. Table includes the water depth at the site, the total number of years of data with 75% data availability, and the years (starting in March of the given year) for which the criterion was met [NDBC; National Oceanic and Atmospheric Administration National Data Buoy Center].

NDBC buoy	Depth (m)	Region	Years	Year list
44025	36	MAB, north	19	1991–1998, 2000–2006, 2008–2010, 2012
44014	48	MAB, south	18	1991–1994, 1996, 1998–2002, 2004–2011
41004	38	SAB, north	16	1994–1995, 1997–1998, 2000–2011
41009	44	SAB, south	23	1989–2011

Table 2
Top 25 storms ranked by Mobility Event Index (MEI; Eq. (3)) for the period 1997–2007. Values under the buoy identification number are the percentage of the total of IWAVES resulting from the storm's mobility event at each site, with the storm ranking (based on IWAVES) at that site in parentheses. If data were available from a buoy during 95% of the time when the storm was causing a mobility event elsewhere (i.e., "storm time"), but a mobility event was not recorded at that site, the site is marked "—". If a mobility event was not recorded and data were available for less than 5% of the storm time, or 5% and 95% of the storm time, the site is marked "n/a" (not available) or "p/a" (partially available), respectively. Asterisks indicate a mobility event where data were available less than 95% of the storm time. Shaded sites are in the MAB. Sites are delineated as the northern (N) or southern (S) site within each region.

Rank	Time period	Type	Name	44025 MAB, N	44014 MAB, S	41004 SAB, N	41009 SAB, S	MEI
1	1999Sep13	TS	FLOYD	–	1.4 (20)	30.2 (1)*	24.9 (1)	0.566
2	1999Aug27	TS	DENNIS	0.4 (63)	13.1 (1)	2.9 (10)*	5.0 (4)	0.213
3	2005Apr15	ETS		0.5 (60)	8.3 (2)	0.1 (37)	6.9 (3)	0.157
4	1998Aug23	TS	BONNIE	1.0 (37)	2.9 (10)	7.9 (4)*	3.4 (9)	0.152
5	2005Jan31	ETS		2.3 (11)	7.7 (3)	1.0 (17)	3.7 (8)	0.147
6	2004Sep02	TS	FRANCES	–	0.2 (45)	8.5 (3)	4.2 (7)*	0.129
7	1999Sep18	TS	GERT	1.7 (17)	6.2 (5)	n/a	4.9 (5)	0.128
8	2001Mar19	ETS		3.6 (5)	2.5 (15)	5.3 (5)	1.1 (17)	0.124
9	2003Sep15	TS	ISABEL	3.0 (8)	n/a	n/a	8.7 (2)	0.117
10	2006Nov21	ETS		3.0 (7)	5.2 (6)	0.9 (18)	0.9 (24)	0.100
11	1998Feb03	ETS		4.5 (3)	n/a	4.4 (6)	0.9 (21)	0.098
12	2004Oct22	ETS		4.6 (2)	4.8 (7)	–	0.3 (46)	0.097
13	2005Sep08	TS	OPHELIA	–	–	9.0 (2)	0.6 (38)	0.097
14	2003Feb16	ETS		3.8 (4)	3.4 (8)	–	p/a	0.072
15	2005Oct12	ETS		7.1 (1)	–	–	–	0.071
16	2004Mar09	ETS		0.0 (86)	6.5 (4)	–	–	0.066
17	2005Oct24	TS	WILMA	2.9 (9)	1.3 (21)	–	1.1 (19)	0.053
18	2002Mar02	ETS		1.6 (19)	1.2 (22)	2.2 (12)	–	0.051
19	2001Sep30	ETS		2.4 (10)	2.4 (16)	–	–	0.049
20	1999Dec01	ETS		n/a	2.6 (13)	–	1.9 (12)	0.045
21	2001Nov05	TS	MICHELLE	–	–	–	4.2 (6)	0.042
22	2000Mar19	ETS		0.5 (58)	2.6 (12)	–	0.7 (32)	0.039
23	2004Sep24	TS	KARL	–	0.3 (42)	3.5 (7)	n/a	0.038
24	1999Apr30	ETS		0.2 (78)	0.8 (27)	1.7 (15)*	1.1 (18)	0.038
25	2005Oct04	TS	TAMMY	–	–	2.9 (11)	0.9 (23)	0.038

on spatial scales of cm (Hurther and Thorne, 2011) to km (Dalyander et al., 2013). To capture the threshold at which most sand grains in a flat bed would be mobilized, a grain-size roughness of 0.35 mm, equivalent to the diameter of medium-coarse sand, was used to calculate τ_w. The presence of ripples and sand waves increases bedform roughness, increasing the total shear stress. The bulk of this increase is from form drag and does not impact sediment mobility (Li, 1994; Rankin and Hires, 2000; Smaoui and Ouahsine, 2012). However, the skin friction will be higher at the crest of the ripple and lower within the trough (Li, 1994). In the case of rippled beds, sand grains within the trough may therefore be immobile under the criterion used here for seafloor mobility, with the threshold instead capturing sediment mobility higher in the ripple profile.

Critical stress values (τ_{crit}) were calculated using the Shields parameter (Shields, 1936, as described in Soulsby, 1997). "Mobility hours" were defined as times when τ_w exceeded 0.2160 Pa, equivalent to τ_{crit} for a 0.35 mm diameter (used as the roughness in calculating τ_w) particle of density 2650 kg/m^3 (quartz sand).

3.2. Identification of Storms

Storm systems that generated waves causing $\tau_w > \tau_{crit}$ were identified using two databases. The National Oceanic and Atmospheric Administration (NOAA) National Hurricane Center (NHC) North Atlantic Hurricane Database (HURDAT 2, National Hurricane Center, 2014) was used to identify TS. This database covers 1851 to present and includes a 6-hourly time-series of the location of minimum low pressure (LP). A database derived from the National Centers for Environmental Prediction (NCEP) and National Center for Atmospheric Research (NCAR) Reanalysis was used to identify ETS (Serreze, 2009). This database includes 6-hourly data of storm LP location for 1958–2008. For each mobility hour, the deep water group wave speed (C_g, in m/s) was calculated following Airy linear wave theory (Airy, 1845; described in Komar, 1998) from peak wave period (T_P, in s) and gravity (g, 9.8 m/s^2):

$$C_g = \frac{gT_p}{4\pi} \quad (1)$$

The calculated arrival time of waves originating from each 6-hourly storm location in the TS database, up to 10 days prior to the time of interest, was compared to the actual arrival time (i.e., the mobility hour). The storm with calculated wave arrival time closest to the mobility hour was chosen as an initial match. If no TS was found with a wave arrival time within 6 h of the mobility hour, the ETS database was checked. The result was a time series of TS or ETS storm IDs for each mobility hour, with gaps where the automated method did not identify a storm. The TS database was checked prior to the ETS database because a TS may transition to an ETS; these storms are in the TS database over all times, and were considered tropical in origin.

Time-series plots of 10-m wind field from the Climate Forecast System Reanalysis (CFSR; Saha et al., 2010) were used to confirm if the correct wave-generating storm had been identified by determining if the storm's wind speed, fetch, angle, duration, location, and timing (accounting for travel time) were consistent with measured waves. Storm IDs were corrected when necessary. Sequential mobility hours with the same storm ID were identified as a "mobility event". Only mobility events lasting longer than 12 h were retained, leaving some mobility hours not associated with a mobility event.

The complexity of weather patterns occasionally made identifying the storm source of an ETS mobility event uncertain. A single LP system can spawn additional LP centers that might re-combine, dissipate, or separate; in other cases, multiple independent LP centers merge. The ETS with the LP cell closest to the center of the wind field identified as generating the waves most responsible for τ_w was selected. If the LP center did not correspond to a storm in the ETS database, it was tagged as an unidentified extratropical

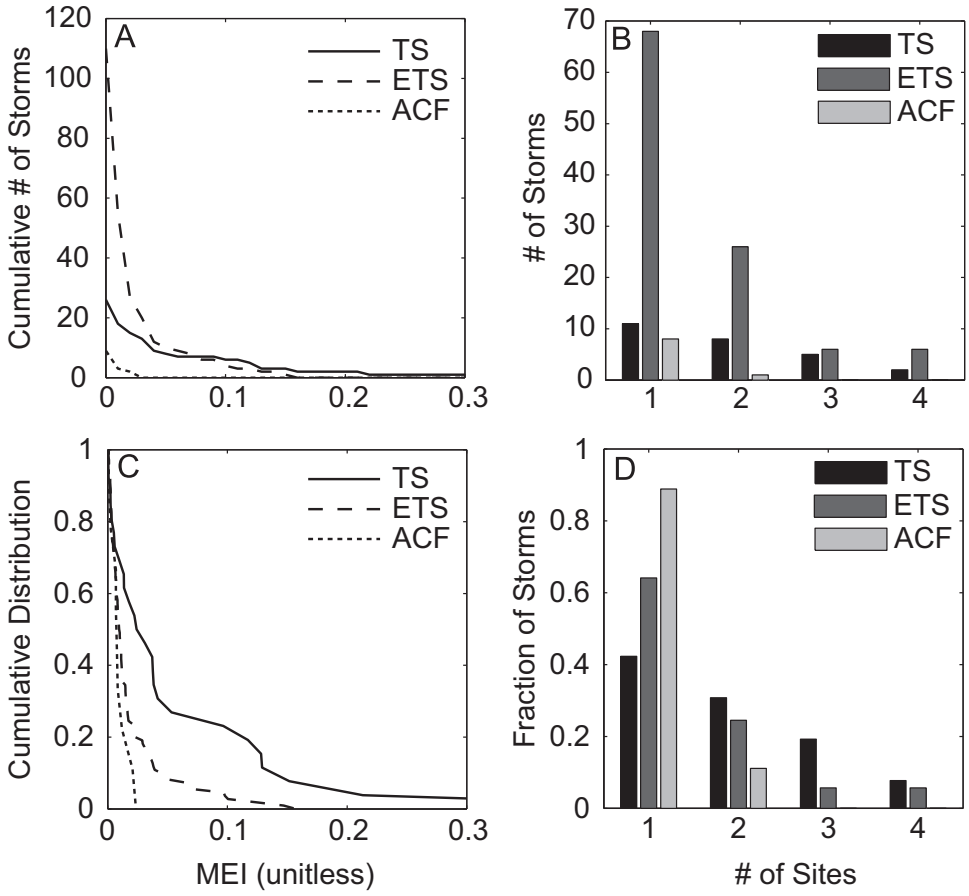

Fig. 2. Number (A) and cumulative distribution (C) of storms (tropical storm, TS; extratropical storm, ETS; anticyclone/front, ACF) exceeding a given value for MEI (Eq. (3)). Sites impacted by number (B) and fraction (D) of each storm type. While there are fewer TS, they affect a larger spatial area (as indicated by number of sites) with greater intensity (as indicated by MEI). The *x*-axis of plots A and C cuts off Hurricane Floyd, with MEI of 0.566 (Table 2). See Table 3 for log-rank *p*-values quantifying statistical difference between the distributions.

Table 3
Log-rank *p*-value comparing the Kaplan–Meier distributions of calculated storm parameters (tropical storm, TS; extratropical storm, ETS; anticyclone/front, ACF). Values indicate the likelihood that the distributions are statistically equivalent; values significant at the 95th percent confidence interval (less than 0.05) are in bold. Distributions for each parameter are shown in the figure indicated. Storm locations and hence distances from site to storm ($D_{\tau w,max}$; $D_{\tau w > \tau w,crit}$) were not calculated for ACF.

Log-rank p	TS, ETS	TS, ACF	ETS, ACF
MEI (unitless); Fig. 2c	**0.001**	**0.012**	0.364
Mean $\tau_{w,max}$ (Pa); Fig. 3d	0.183	**0.016**	**0.029**
Max $\tau_{w,max}$ (Pa); Fig. 3e	**0.015**	**0.006**	**0.010**
Mean duration (hours); Fig. 3f	**0.019**	**0.125**	0.831
Mean $D_{\tau w,max}$ (km); Fig. 4c	**0.012**	–	–
Mean $D\tau_w > \tau_{w,crit}$ (km); Fig. 4d	**0.000**	–	–

storm (uETS). Mobility events could also be tagged as an anticyclone or front (ACF) if the winds driving the mobility-inducing waves did not result from counterclockwise rotation around a LP center.

3.3. Quantification of storm strength

Mobility event strength was quantified with the Butman et al. (2008) IWAVES metric, which incorporates the magnitude and duration of a mobility event. IWAVES was calculated by subtracting τ_{crit} from τ_w, resulting in a time-series of "excess" stress. Excess stress was set to zero when τ_w was less than τ_{crit}, then integrated over the duration of the event to obtain a single IWAVES value, in Pa h.

$$\text{IWAVES} = \sum_{\text{stormtimes}} \max(\tau_w - \tau_{crit}, 0) \quad (2)$$

The Mobility Event Index (MEI) was defined to rank a storm's shelf-wide impact (Table 2).

$$\text{MEI} = \sum_{\text{sites}} \frac{\text{IWAVES}_{\text{storm,site}}}{\sum_{\text{storms}} \text{IWAVES}_{\text{site}}} \quad (3)$$

IWAVES for each mobility event at each site ($\text{IWAVES}_{\text{storm,site}}$) was normalized by the total IWAVES summed over all mobility events at that site ($\text{IWAVES}_{\text{site}}$) so MEI was not biased by sites with greater overall mobility. In some cases one or more buoys were not reporting data during the entirety of a mobility event, resulting in an under-prediction of MEI.

4. Results

4.1. Relationship of seafloor mobility to storm Characteristics

A total of 145 storms generated waves resulting in mobility events at one or more sites between March 1997 and March 2007. Of these storms, 8 result in mobility events at all 4 sites; 11 at 3 sites; 35 at 2 sites; and 91 at 1 site (Fig. 2). Of the 145 storms, 106 (73%) were identified in the ETS database, 26 (18%) were identified in the TS database, 9 (6%) were associated with ACF, and 4 (3%) were associated with uETS. ACF and uETS typically drove mobility

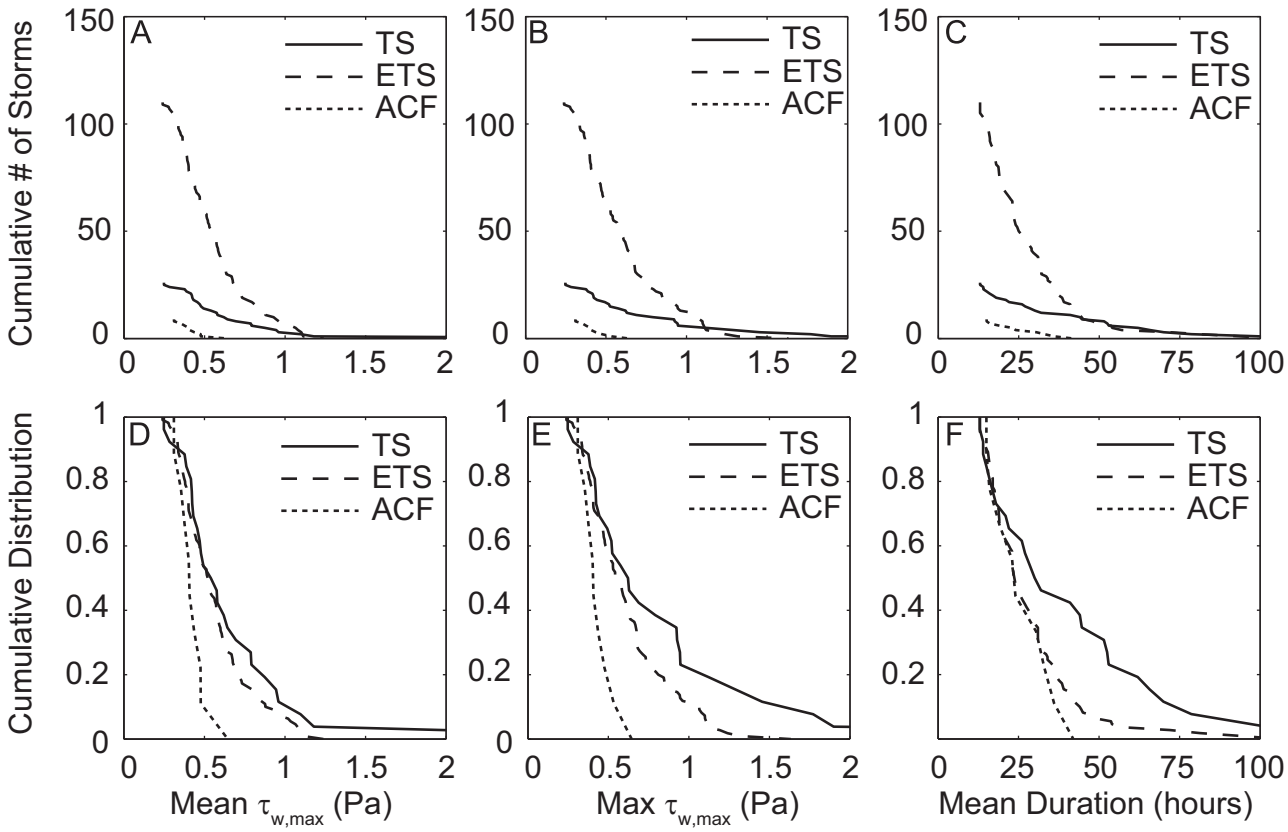

Fig. 3. Number (A, B, C) and cumulative distribution (D, E, F) of storms by type (tropical storm, TS; extratropical storm, ETS; anticyclone/front, ACF) resulting in exceedance of a given value of mean $\tau_{w,max}$, maximum $\tau_{w,max}$, and mean duration. $\tau_{w,max}$ is the maximum skin friction resulting from the storm at any site where it drove a mobility event; mean and maximum for each storm were calculated from $\tau_{w,max}$ values at each site. Mean and maximum were only calculated for those sites where a mobility event was identified. Similarly, duration was calculated for each storm's mobility event at each site, with the mean value for the storm calculated as the average of the values from each site where the storm drove a mobility event. TS are more intense (higher $\tau_{w,max}$) and of longer duration than ETS or ACF. See Table 3 for log-rank *p*-values quantifying statistical difference between the distributions.

events at a single site that were of shorter duration (on average 27 and 24 h) compared to TS (impacting an average of 1.9 sites with a mean duration of 41 h) and ETS (impacting an average of 1.5 sites with a mean duration of 29 h).

Of the 25 largest storms ranked by MEI 14 were ETS and 11 were TS (Table 2). Individual TS accounted for 2–30% of total IWAVES at the SAB locations and 0.4–13% of total IWAVES at the MAB sites. Individual ETS tended to contribute a smaller percentage of IWAVES than TS, accounting for a maximum of 8% of IWAVES at any given site. Hurricane Floyd was the largest storm, primarily caused by large IWAVES at 41004 and 41009. The two highest ranked ETS occurred in April and January of 2005. The total IWAVES was 316 Pa h, 250 Pa h, 273 Pa h, and 428 Pa h at 41004, 41009, 44014, and 44025, respectively, with Floyd accounting for 30% and 25% of IWAVES at 41004 and 41009 (Table 2).

Distributions of the total number of storms of each type vs. exceedance values of MEI, number of sites impacted, and distance from storm to sites where mobility events occurred were used to contrast the effects of TS and ETS on seafloor mobility. A Kaplan–Meier (K–M) estimator (Kaplan and Meier, 1958) was applied to the data to create a complimentary cumulative distribution function (also known as the survival or reliability function; this function determines the likelihood of the parameter of interest exceeding a given value). The log-rank value (Mantel 1966; Berty et al., 2010) was calculated to determine if the difference in K–M distribution between ETS and TS (or ACF) was statistically significant (Table 3). ETS and TS resulted in mobility events observed at all four sites and with high values of MEI (Fig. 2). More ETS (Fig. 2A and B) drove mobility events than TS; however, their individual impact tended to be small (MEI less than 0.05 for over 90% of ETS) and confined to a smaller area (over 60% of ETS resulted in mobility events at a single site). TS had the largest values of MEI and a larger fraction of TS drove mobility events across a broader spatial area (2 or more sites). Only a single ACF impacted two sites in the SAB, while the other eight registered as mobility events at only one site and had a low MEI.

The maximum stress driven by a storm ($\tau_{w,max}$) and the duration of its mobility events were also used to quantify TS and ETS (Fig. 3). The magnitude of $\tau_{w,max}$ was larger for most TS than for ETS; the difference in TS vs. ETS distributions of maximum $\tau_{w,max}$ at a single site was significant at the 95% confidence interval, while the difference in TS vs. ETS distributions of mean $\tau_{w,max}$ at all sites where the storm was observed was not significant (Table 3). TS resulted in longer duration events, calculated as the mean duration over all impacted sites (Fig. 3; Table 3) and as the longest duration at a single site (not shown). The duration of individual TS events was found to be extended by far-field swell of varying T_p generated at the same time arriving over a span of hours to days. ACF produced smaller values of $\tau_{w,max}$ than TS and ETS, while the duration of ACF events exhibited a similar distribution to ETS (Fig. 3; Table 3).

The distance between each site and the storm's LP center at the time of wave generation resulting in $\tau_{w,max}$ was determined ($D_{\tau w,max}$) and the mean calculated for all impacted sites (mean $D_{\tau w,max}$; Fig. 4A and C). The mean of the maximum distance from which each storm produced waves resulting in mobility ($D_{\tau w > \tau crit}$) was also calculated over all impacted sites (Fig. 4B and D). The average distance of TS to impacted sites was 2000–3000 km when waves

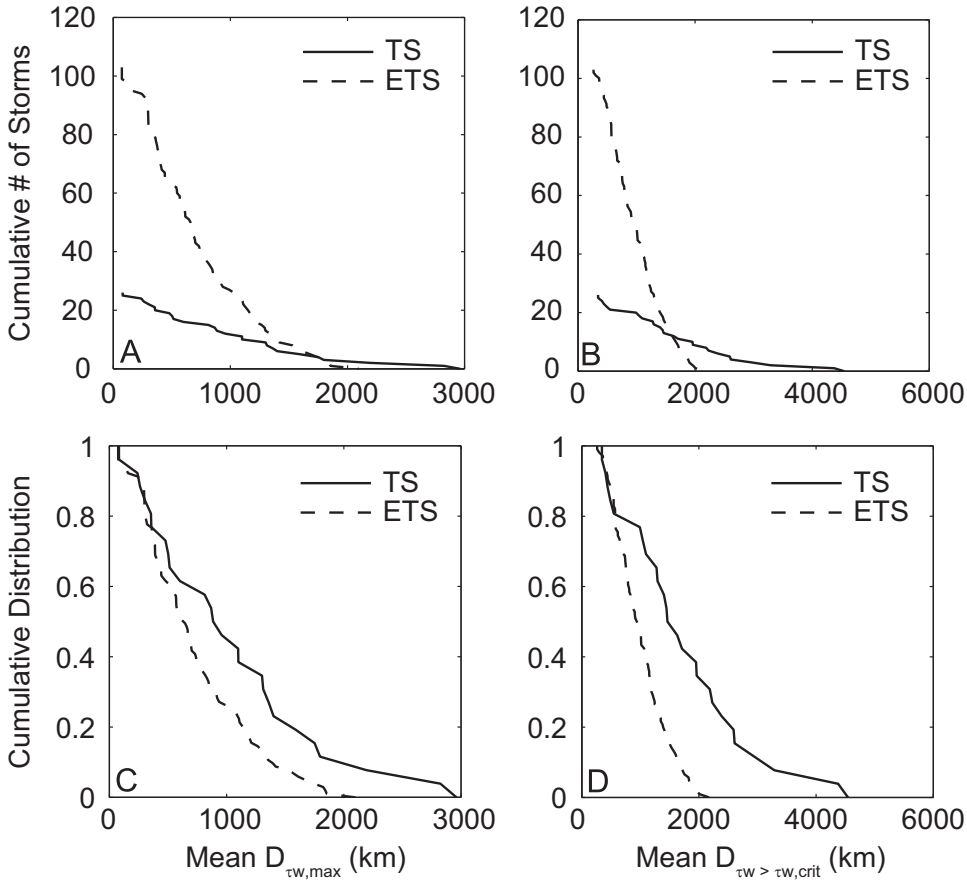

Fig. 4. Number (A, B) and cumulative distribution (C, D) of storms by storm type exceeding a given value of mean $D_{\tau_{w,max}}$, the distance from the sites to the storm when waves generated the maximum stress were generated, averaged over all impacted sites; and mean $D_{\tau w > \tau crit}$, the distance from the sites to the storm when waves resulting in mobility threshold exceedance were generated from farthest away, averaged over all impacted sites. See Table 3 for log-rank *p*-values quantifying statistical difference between the distributions.

producing $\tau_{w,max}$ were generated, and TS generated mobility threshold exceedance at distances of up to 4000 km. In contrast, ETS drove mobility events at sites less than 2000 km away.

4.2. Spatial variability in mid-shelf seafloor mobility response

The statistics of mobility events varied depending on location (northern and southern parts of the MAB and SAB) and water depth (Table 4). The percentage of mobility hours within mobility events ranged from 71% to 88%; the remainder occurred in intervals less than the 12 h criteria. The highest percentage of non-event mobility hours occurred at the northern SAB site (41004). Mean event duration ranged from 1.3 to 1.7 days, with slightly longer events at the deeper water depths. Mean distance to storm LP center ranged from ~800 to 1100 km, and was higher at the deeper sites in the MAB and SAB. LP storm centers influencing the SAB sites were ~200 km further away than for MAB sites. Mean IWAVES was highest at the northern SAB site, caused by fewer, generally more intense mobility events compared to the other sites.

In the MAB, ETS and uETS accounted for a larger percentage of mobility hours and a higher fraction of IWAVES than TS did (Table 5). In the SAB, ETS and uETS accounted for approximately the same percentage of mobility hours as TS, but the greater intensity of TS resulted in a higher fraction of IWAVES coming from TS. In contrast to the MAB sites and the northern SAB site (41004), where ACF made negligible contributions to mobility hours and IWAVES, ACF accounted for 11% of mobility hours and 8% of IWAVES at the southern SAB site (41009). Davis et al. (1993) identified

Table 4
Characteristics of mobility events identified at sites in the MAB (shaded) and SAB (unshaded) over the time period of 1997–2007. Depth is the water depth (in meters, m). Other values given are as follows: mobility, the mean and standard deviation of the number of days of mobility each year; event mobility, the mean and standard deviation of the percentage of time each year when mobility threshold exceedance was within a 12+ h mobility event; events/yr, the mean and standard deviation of the number of mobility events per year; event duration, the average length of time of mobility events; Distance, the average distance between the buoy and the LP center of the storm generating the waves driving mobility; and IWAVES, average IWAVES over all storms as calculated in Eq. (2).

Buoy	Depth (m)	Region	Mobility (days/yr)	Event mobility (%)	Events/yr (yr^{-1})	Event duration (days)	Distance (km)	IWAVES (Pa h)
44025	36	MAB, N	12.3 ± 4.5	79 ± 13	8.9 ± 3.7	1.3	824	4.9
44014	48	MAB, S	8.9 ± 5.0	79 ± 11	5.4 ± 3.5	1.6	966	5.7
41004	38	SAB, N	6.1 ± 3.4	71 ± 18	4.0 ± 1.5	1.4	1073	7.9
41009	44	SAB, S	7.3 ± 4.1	88 ± 9	5.0 ± 2.1	1.7	1128	5.0
Avg	42		8.6 ± 4.2	79 ± 13	5.9 ± 2.7	1.5	998	5.9

Table 5
Percentage of mobility hours (h) and percentage of IWAVES for each site attributable to tropical storms (TS), extratropical storms in the ETS database (ETS), extratropical storms not in the ETS database (uETS), and anticyclones or fronts (ACF). Also given is the percentage of mobility hours not associated with a 12 plus hour mobility event (NE). Shaded rows indicate sites in the MAB, unshaded rows indicate buoys in the SAB. Sites are delineated as the northern (N) or southern (S) site within each region.

Buoy	Depth (m)	TS		ETS		uETS		ACF		NE	
		Hrs (%)	IWAVES (%)	Hrs (%)	IWAVES (%)	Hrs (%)	IWAVES (%)	Hrs (%)	IWAVES (%)	Hrs (%)	IWAVES (%)
44025 MAB, N	36	12	11	67	87	2	2	1	0	18	-
44014 MAB, S	48	21	33	61	67	0	0	0	0	18	-
41004 SAB, N	38	34	67	40	33	1	0	1	0	24	-
41009 SAB, S	44	41	66	36	25	1	1	11	8	11	-

anticyclones as generating sufficiently energetic waves to drive coastal change, and Warner et al. (2012) found that frontal systems affected mobility in water depths of 10 m. Our result indicates ACF also generate sufficiently energetic longer period swell to result in seafloor mobility at mid-shelf depths (44 m) in parts of the SAB.

A storm's location may be identified by the LP center (Fig. 5), but the associated wind field may extend over 10's–100's of km. At 44025 (northern MAB), the LP centers of ETS driving mobility were located to the east and west of the buoy and as far south as 30°N, while TS driving mobility were located to the east and as far south as 20°N. Mobility at 44014 (southern MAB) was driven by ETS to the east and south as far as 30°N, with fewer storms to the west. TS driving mobility at 44014 had a similar spatial distribution to 44025.

In the SAB, the location of TS and ETS driving mobility events was distinctly different than for the MAB (Fig. 5). For 41004 (northern SAB), ETS were located to the east and west, and as far south as 25°N, while TS driving mobility events were predominantly confined to locations SE of the buoy. For 41009 (southern MAB), ETS generating mobility events were predominantly offshore to the E and NE. The location of TS driving

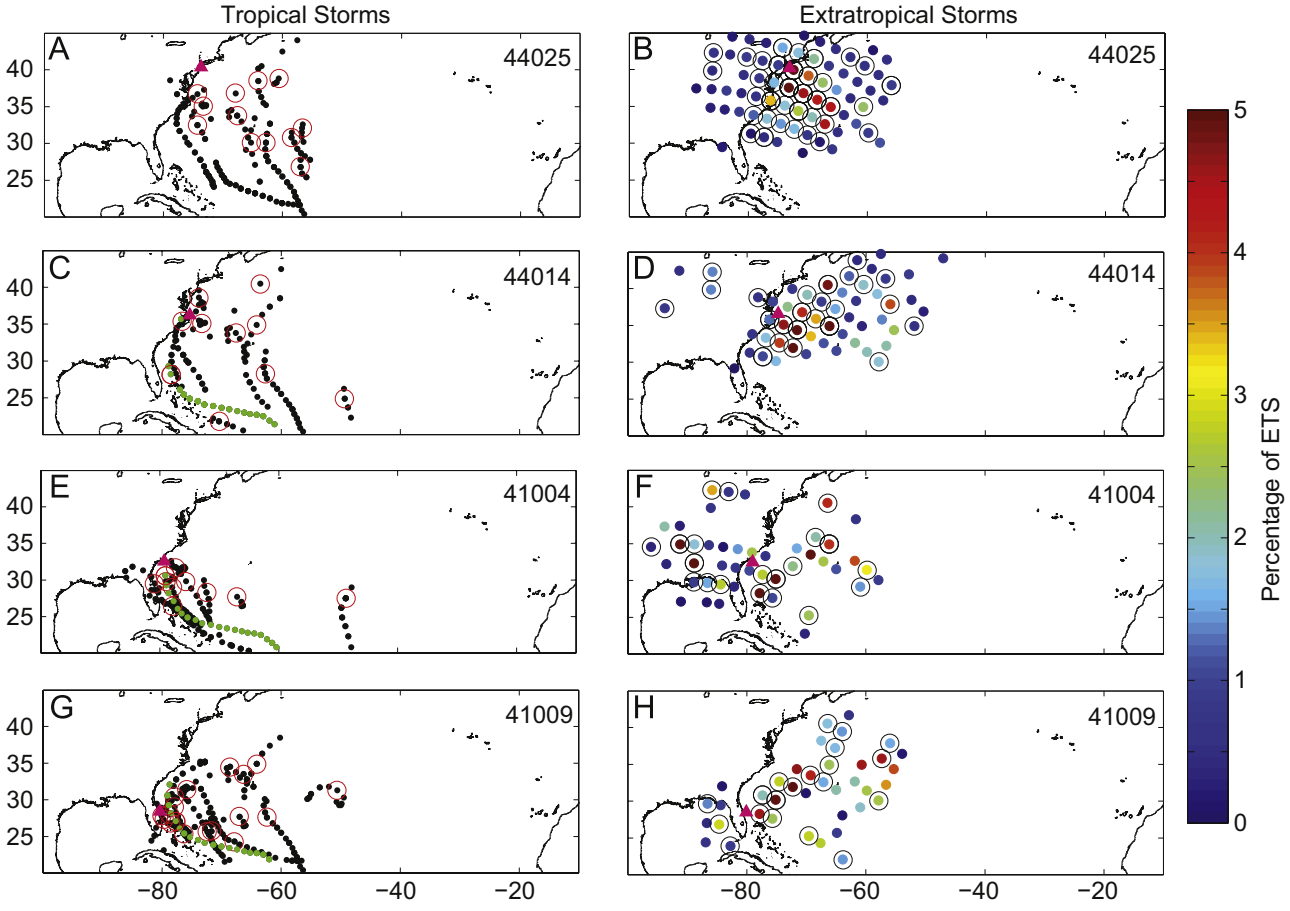

Fig. 5. Location of the low-pressure center of tropical (TS, left four panels) and extratropical (ETS, right four panels) storms at the time waves were generated that drove mobility events at 44025 (A,B), 44014 (C,D), 41004 (E,F), and 41009 (G,H). Buoy locations are marked by pink triangles. The storm locations are hours to days prior to the time mobility events were observed at the sites. For TS, the black (green for Hurricane Floyd, see Fig. 7) dots show locations where waves were generated that resulted in mobility hours and the red circles indicate the location where waves were generated that resulted in the maximum bottom stress for that storm. Because the ETS database is based on numerical model output and storm locations are therefore confined to the locations of the model grid points, plotting the location of all event generating storm locations individually would result in an indistinguishable overlapping pattern. Therefore, the percentage of mobility hours at each buoy resulting from each possible ETS LP location is shown, and locations where the waves driving maximum bottom stress originated for at least one storm are circled.

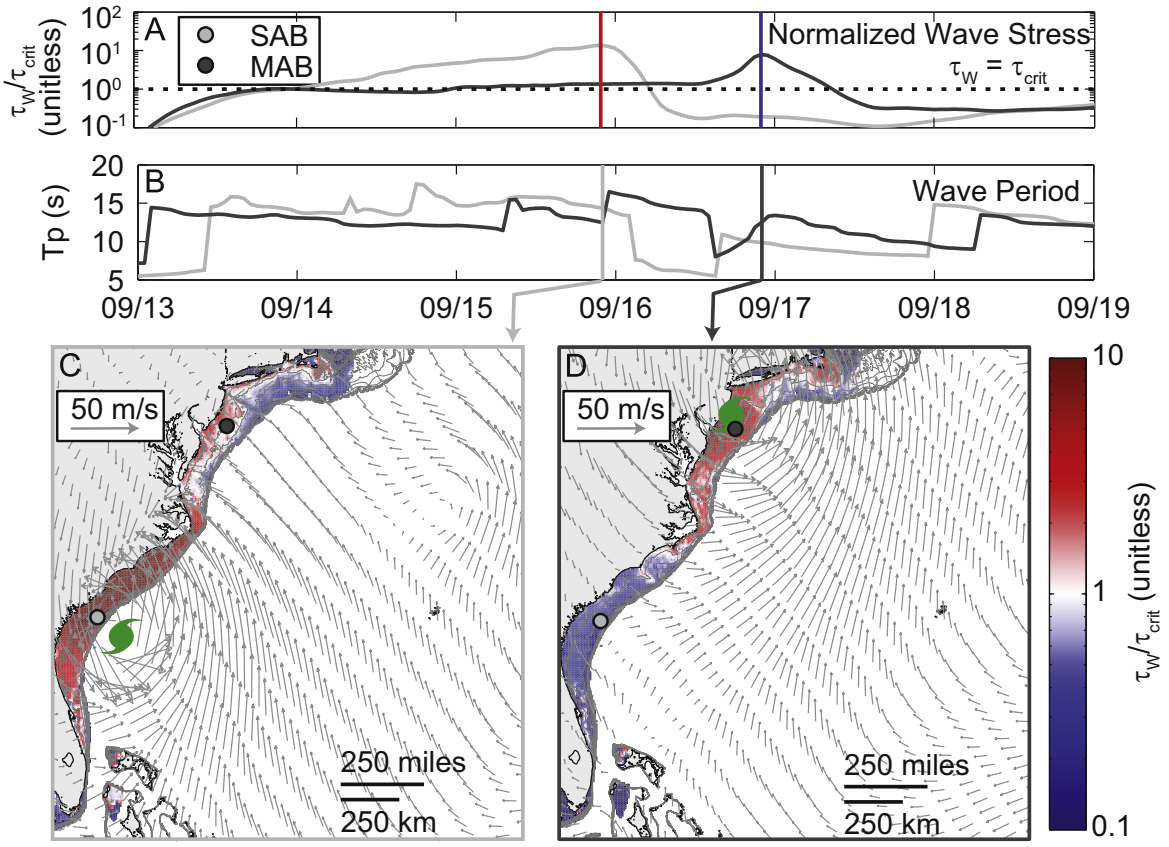

Fig. 6. Time series of τ_w/τ_{crit} (A) and peak wave period (B) at one location in the SAB (light gray dot and time series) and one in the MAB (dark gray dot and time series) during Hurricane Floyd in September of 1999. Water depth at both sites is 40-m. A ratio of τ_w/τ_{crit} greater than one indicates mobility threshold exceedance. Maps (C, D) show τ_w/τ_{crit} at 2200 on 9/15 and at 2200 on 9/16 (times marked by light and dark gray lines in A and B). Arrows are wind vectors at 10 m. In (C) and (D), red indicates mobility threshold exceedance, and blue indicates no mobility. In both (C) and (D) the storm center was close to the coast and swell propagation time to the closest buoy would be negligible; however, mobility in regions farther from the storm is caused by waves generated hours earlier.

Table 6
Table of buoys in the Middle Atlantic Bight (MAB) and South Atlantic Bight (SAB) used in long-term, large scale mobility occurrence analysis. Table includes the water depth at the buoy, the total number of years of data with 75% data availability, and the years (starting in March of the given year) with sufficient data coverage.

Buoy	Depth (m)	Region	Years	Year List
44017	45	MAB	8	2003–2010
44009	28	MAB	23	1987–1991, 1995–2012
41025	68	SAB	7	2003, 2005–2010
41036	31	SAB	5	2007–2009, 2011–2012
41013	24	SAB	8	2004, 2006–2012
41008	18	SAB	20	1988–1991, 1997–2012
41012	37	SAB	8	2004–2006, 2008–2012

mobility events at 41009 had a similar pattern to 41004, but extended farther to the NE offshore of the MAB.

4.3. Hurricane Floyd

Patterns in bottom stress associated with Hurricane Floyd, the strongest storm identified during March 1997–March 2007 (Table 2), illustrates the differences in seafloor mobility in the SAB and MAB that can be caused by the same storm. The WAVEWATCHIII® numerical wave model (Tolman, 2007, 2009) was used to simulate waves for 13-19 September 1999. A nested 3-grid setup employing the operational WAVEWATCHIII® 30′ global, 10′ northwest Atlantic, and 4′ U.S. East Coast model domains was used (Chawla et al., 2007), with wind forcing provided by CFSR winds (Saha et al., 2010). Hourly values of u_{br} and T_{br} were used to calculate τ_w with the same 0.35 mm grain size roughness used for buoy analysis. A new model run was required because archived WAVEWATCHIII® output does not include u_{br} and T_{br}, and errors in model T_p introduce large errors in calculated τ_w when using the parameterized spectrum approach. The model was assessed against buoy measurements and performed with good skill (mean root-mean square error for the four buoys of 0.3 m, 1.9 s, and 0.1 Pa, and normalized root-mean square error of 0.03, 0.09, and 0.05, for significant wave height, T_p, and τ_w, respectively).

Hurricane Floyd was a Cape Verde storm that approached the SAB from the southeast (Lawrence et al., 2001). Long-period swell arriving ahead of the storm resulted in mobility threshold exceedance at the SAB site on September 14, when the storm was still far from the coast, and slight exceedance of mobility threshold in the MAB on September 15 (Fig. 6A and B). A peak in τ_w occurred at values up to 10 times τ_{crit} when the storm was located near the SAB site (Fig. 6C). At the same time, swell reaching the MAB drove mobility threshold exceedance on the inner- and mid-shelf. As the storm moved to the north (Fig. 6D), τ_w in the MAB continued to increase, while in the SAB τ_w dropped below τ_{crit} on September 16.

Storms located offshore of the SAB are positioned such that winds in the powerful northeast quadrant generate waves directed from the SAB north toward Cape Cod (Figs. 5 and 6), causing elevated τ_w along the entire U.S. East Coast. In contrast, winds from storms just offshore of the MAB region are aligned such that the most powerful swell is directed toward the north and west, and do not generate waves that propagate into the SAB with sufficient energy to drive mobility events. The response at site 41009 vs.

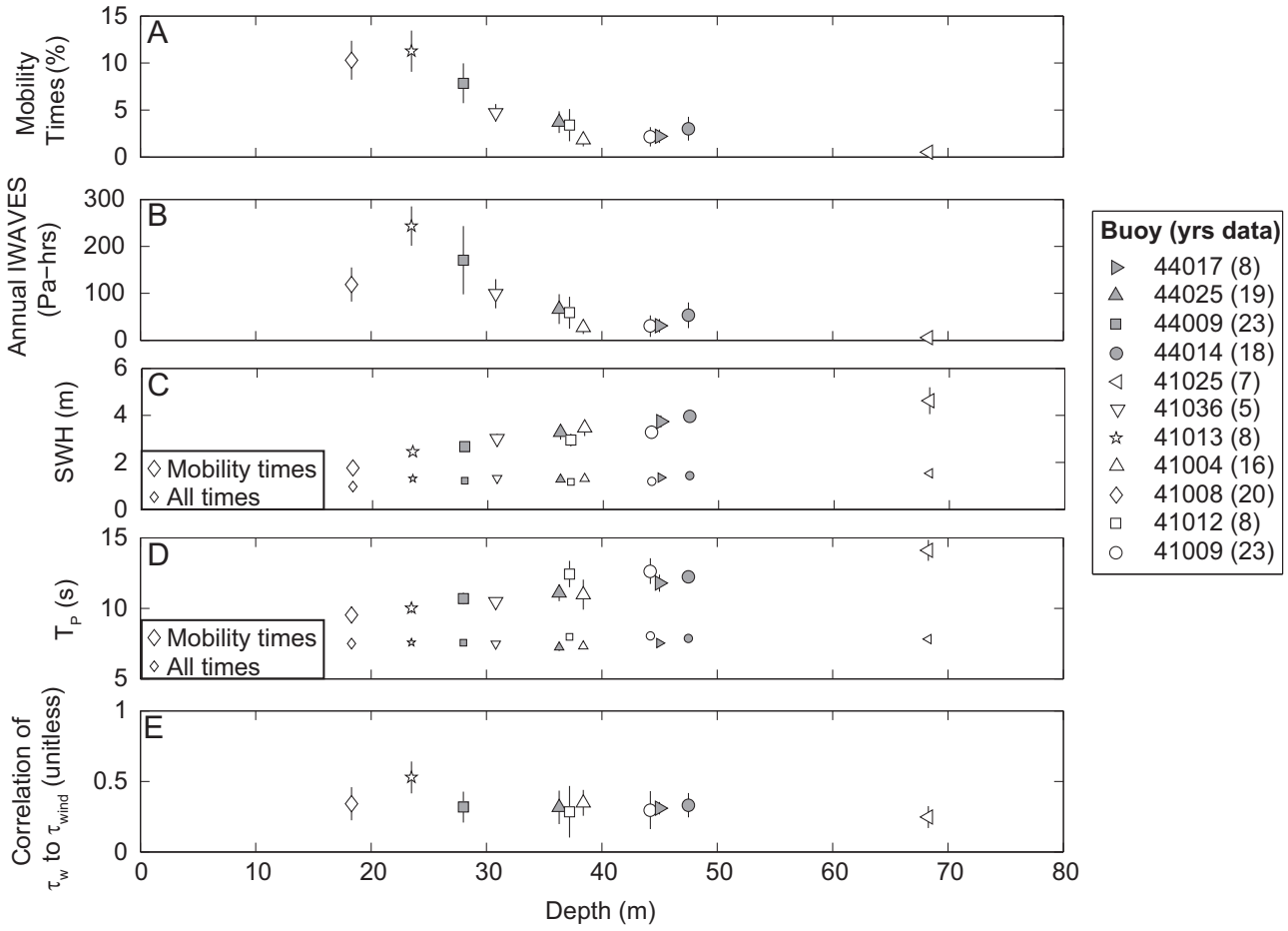

Fig. 7. Percentage of mobility hours (A), total annual IWAVES (B), peak wave period (T_P; C), significant wave height (SWH; D), and correlation of wave stress (τ_w) to wind stress (τ_{wind}) (D) vs water depth at the NDBC buoy sites (Fig. 1). In (C) and (D), larger symbols indicate the T_P and SWH average over mobility hours, smaller symbols indicate average over all times. The symbol marks the mean and the vertical bar one standard deviation of values for all years having greater than 75% temporal coverage for that year. Percent mobility and IWAVES decrease with water depth, while the peak wave period during mobility hours increases with depth. Correlation between local wind and wave stress is less than 0.50 at all sites.

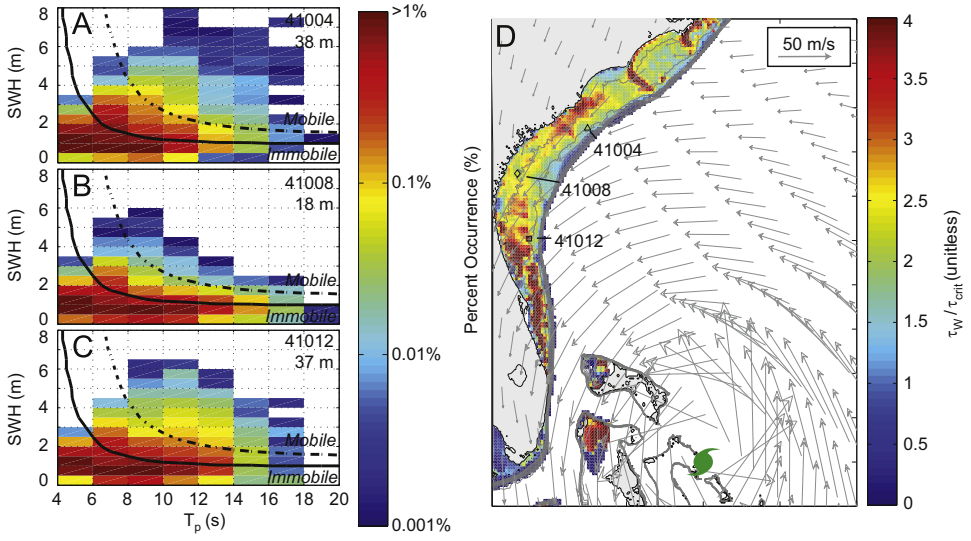

Fig. 8. Percent occurrence of significant wave height (SWH) and peak wave period (T_p) at South Atlantic Bight (SAB) sites 41004 (A), 41008 (B), and 41012 (C) for 1997–2007 (note log scale). Shown are the thresholds for mobility of 0.35 mm sediment assuming a JONSWAP surface wave spectrum in 18 m water depth (solid black line) and 37 m water depth (dot–dashed black line). The map (D) shows τ_w/τ_{crit} (color scale) for numerical model output at 1000 on 9/14/99, when Hurricane Floyd (green hurricane symbol) was to southeast of the SAB. A ratio of τ_w/τ_{crit} greater than one indicates mobility threshold exceedance. Gray vectors show wind speed and direction. (For interpretation of the references to color in this figure legend, the reader is referred to the web version of this article.)

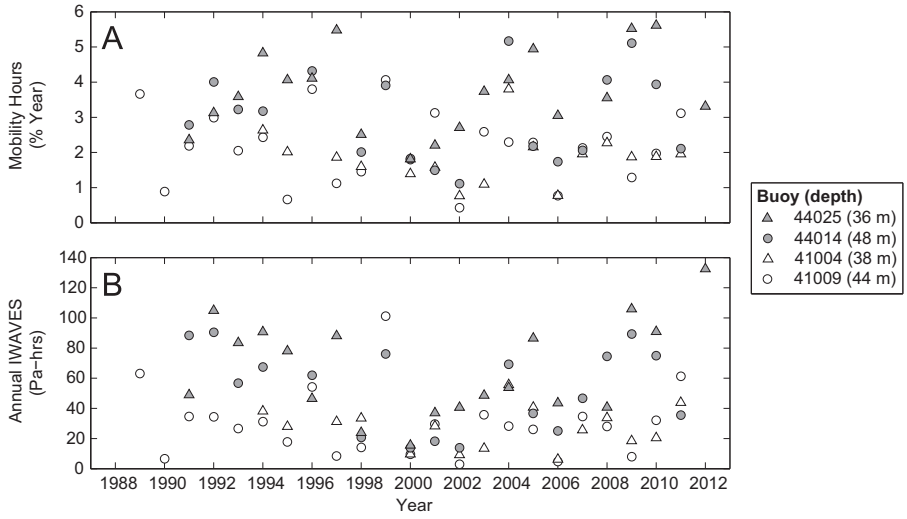

Fig. 9. Percentage of mobility hours (A) and total annual IWAVES (B) for sites in the SAB (open symbols) and MAB (gray symbols) for years (March to March) 1988–2012. Triangles denote buoy sites in water 36–38 m deep and the circles denote buoys in water 44–48 m deep. All years displayed have greater than 75% data coverage for that year. Annual values of % mobility and IWAVES range by a factor of ~10 and sites in the MAB typically have higher values than in the SAB.

41004 to swell propagating from storms somewhat farther offshore of the MAB indicates that locations offshore and south of Cape Canaveral may receive swell driving mobility events from storms in these locations (Fig. 5), whereas the rest of the SAB is shielded from these waves by Cape Hatteras.

4.4. Shelf-wide seafloor mobility

Mobility occurrence was analyzed at seven additional buoy sites (Table 6; Fig. 1) to investigate variability over a wider range of water depths, area, and time. Mean T_P was between 6 and 8 s, whereas mean T_P when $\tau_w > \tau_{crit}$ was 9–14 s and increased with depth (Fig. 7). Mean significant wave height (SWH) was 1–2 m over all times and 2–4 m, increasing with depth, when $\tau_w > \tau_{crit}$ (Fig. 7). The mean correlation between τ_w and wind stress was low (0.25–0.53); in contrast, the correlation between SWH and wind stress was 0.65–0.80. These results are consistent with the conclusion that at these water depths (18–70 m), as in the case of the four mid-shelf sites, energetic swell from the far-field dominated seafloor mobility. A study in Massachusetts Bay (Fig. 1) found the largest IWAVE events came from ETS that ranked high by a metric of local wind stress (Butman et al., 2008). The correlation with local winds, higher than found here, is attributed to the fact that the bay is a semi-enclosed basin, and local winds were likely well-correlated to the large scale winds characteristics of ETS.

Percentage of mobility hours and annual IWAVES generally decreased with increasing water depth (Fig. 7), except at 41008 in 18 m depth in the central SAB. Possible reasons for the lower values of IWAVES at 41008 include wave energy increase between the shallow and deep sites due to offshore winds; wave refraction, as 41008 is 110 km from the shelf break in the central SAB; swell wave attenuation, which can be significant during storms (Ardhuin et al., 2003); or temporal differences in the wave climate. Given that waves generating mobility events were identified as originating from far-field storms, it is unlikely that local winds are the driving factor. Comparison of SWH and T_p distribution at 41008 to 41012 (155 km to the south in 37 m of water) and 41004 (207 km to the north in 38 m of water) shows that long-period swell of sufficient energy for mobility occurred less frequently at 41008 than at the deeper sites (Fig. 8A–C). Numerical model output from September 14, 1999 at 1000, when Hurricane Floyd was southeast of the SAB, show a complex pattern of τ_w (Fig. 8D). Modeled and observed T_p values (Fig. 6) from Cape Canaveral north to Cape Hatteras (Fig. 1) were 12–17 s coming from the south-southeast, consistent with swell from Floyd. Depressed values of τ_w in the central SAB compared to similar depths to the north and south suggest the influence of wave refraction (Fig. 7). In addition, where the shelf is wide, model output shows a mid-shelf maximum in τ_w likely as a result of wave attenuation due to bottom friction (Fig. 8D). The numerical model output and buoy analysis suggests that the depressed mobility at 41008 (Fig. 7) is the result of wave refraction and swell attenuation over the wide shelf in the central SAB, although cross-shelf observations of τ_w and mobility would be required to confirm these findings.

5. Discussion

5.1. Sensitivity to sediment grain size

Grain size along the U.S. East Coast varies on meter to kilometer scales, which affects τ_w and τ_{crit}. The sensitivity of mobility predictions to grain size was quantified by comparing the baseline value of 0.35 mm to values of 0.45 mm and 0.09 mm, representing plus and minus one standard deviation around the median grain size in 30–50 m water depth offshore of the U.S. East Coast. The percentage of mobility hours for 1997–2007 differed by 8–15% of the baseline values for the 11 buoys (1, 6), with higher mobility percentages for the smaller grain size and lower mobility percentages for the larger grain size. For the purposes of identifying seafloor mobility and the storms driving mobility events over the bulk of the shelf where sand is the dominant component, the single value of 0.35 mm was deemed sufficient.

5.2. Other contributions to seafloor mobility

Near-bottom currents not associated with waves can contribute substantially to seafloor mobility. For example, analysis of numerical model output indicated that strong tidal currents were sufficient to induce mobility in the Nantucket Shoals region (Fig. 1; Dalyander et al., 2013). Throughout the rest of the MAB, Dalyander et al. (2013) found that non-tidal currents contributed to wave-current shear stress in depths less than approximately 40 m, as well as in the deeper Hudson Shelf Valley (Fig. 1). That study did not account for internal waves, which occur in the MAB in summer and can result in sediment resuspension (Butman et al., 1979;

Churchill et al., 1994). Surface waves are often the primary force mobilizing sediment, subsequently transported by currents, as was found offshore of New Jersey (Fig. 1) during Nor'Ida, a hurricane that transitioned into an ETS as it moved up the U.S. East Coast (Miles et al., 2013). The duration of mobility will likely be controlled by waves, as was observed offshore of North Carolina (Fig. 1), where ETS were found to have an extended period of sediment suspension corresponding to the arrival of far-field swell from the retreating storm (Kim et al., 1997). Similarly, modeling of TS Floyd offshore of New Jersey (Fig. 1) determined that near-bottom currents in 12 m of water peaked at 10–20 cm/s during the height of the storm, but were considerably lower (few cm/s) when the storm was not local to the site (Kohut et al., 2006).

Another potential driver of seafloor mobility is infragravity motion. These waves have periods longer than 20 s (Munk, 1949; Tucker, 1950), and originate via non-linear interactions (Hasselmann, 1962; Longuet-Higgins and Stewart, 1962, 1964) or energy transfer to lower frequency waves through a time-dependent wave breaking point (Symonds et al., 1982). Infragravity waves can be bound to shore, or radiate out to deeper water (Herbers et al., 1994, 1995a, 1995b). Infragravity wave energy can dominate the surf zone and be significant ($> 100\ \mathrm{cm}^2$) at inner shelf depths of < 20 m (Herbers et al., 1994; Ruessink, 1998). The amplitude of infragravity waves has an inverse relationship to depth, reducing to $O(10^{-2}\ \mathrm{m})$ in the deep Atlantic (Aucan and Ardhuin, 2013), therefore the contribution to seafloor mobility at the mid-outer shelf is likely small compared to the inner shelf and surf zone.

At shallow depths (< 10 m), shear stress may depend on wave skewness (Elfrink et al., 2006); however, this effect is expected to be minimal for waves and particularly swell over the shelf. Values of u_{br} and T_{br} calculated using linear wave theory and an assumed spectral shape were assessed against observations of near-bottom currents in depths of 30–60 m by Wiberg and Sherwood (2008) and Butman et al. (2008), with resultant error generally less than 10%.

5.3. Interannual variability and climate change implications

To determine the representativeness of the study period, the number and spatial distribution of storms was determined by counting the number of occurrences of LP centers of each type in 5° x 5° grid cells covering the U.S. East Coast (-90°W to 50°W and 20–45 °N). The frequency of storms for 1997–2007 was compared to the 1958–2008 period covered by the ETS database. The spatial distribution of TS and ETS for the study period was similar to the 50-year record; however, storm activity was higher than average. There were 28% more TS hours/year during 1997–2007 (2083 TS h/year) than for 1958–2008 (1628 TS h/year), and 7% more ETS hours/year during 1997–2007 (8927 ETS h/year) than for 1958–2008 (8310 h/year). The percentage of annual mobility hours and IWAVES at mid-shelf depths varied by factors of six and ten over the period of 1988–2012, respectively, with the MAB sites tending toward higher values than the SAB (Fig. 9). This suggests that although year-to-year variation in the types and tracks of storm will introduce variability, the combined effect of far-field swell from TS and more local ETS in the MAB results in persistently more mobility in the MAB than in the SAB at similar mid-shelf depths, and the 1997–2007 time period is representative of this phenomena despite being more active in terms of storms than the 50 year period of 1958–2008.

Storm patterns may evolve with climate change, although there is uncertainty in the type and magnitude of any shift and how it would compare to historic decadal variability (Kirtman et al., 2013). Possible changes include a reduction in the number of ETS or TS, more intense storms, and a shifting of storm tracks poleward (Bengtsson et al., 2006). An increase in a storm's intensity will increase the maximum induced τ_w. An additional effect may arise through changes in T_p; stronger storms can produce swell that survives dissipation over greater distances, thereby resulting in a greater number of storms that generate τ_w events on the mid to outer shelf. In contrast, greater attenuation of longer period swell through bottom friction may reduce the wave energy reaching the inner shelf. Changes in storm track would also impact seafloor mobility. For example, if storm tracks shift poleward, fewer storms would pass to the southeast of the SAB, where waves capable of impacting the entire U.S. East Coast shelf now originate, resulting in fewer mobility events along the entire coast and particularly in the SAB.

5.4. Implications for numerical modeling

The findings of this study have ramifications for accurate numerical model prediction of seafloor mobility, as well as other processes (such as wave runup) where swell waves contribute significantly. A model domain extending approximately 2000 km from any of the four sites considered would capture waves generated by all of the ETS driving sediment mobility over the period of 1997–2007, but a domain of that size would exclude approximately half of the TS (Fig. 4D). In cases where a nested grid approach is used, application of full wave spectra on the boundaries, such as done here for Hurricane Floyd (Section 4.3), may be needed to accurately capture swell propagating into the domain, particularly in cases of bi-modal wave distribution.

6. Summary

This study used observations of surface waves at NDBC buoys to identify when wave-driven seafloor mobility events likely occurred at depths of 35–50 m along the U.S. East Coast during March 1997–March 2007. Mobility events were gaged by intensity, duration, and IWAVES (combined metric).

Storms located hundreds to a few thousand km away, particularly tropical cyclones due to their high wind speeds, were significant drivers of mid-shelf mobility events. Of the 25 largest mobility events, 14 were ETS and 11 TS, based on a Mobility Event Index (MEI) that ranks the relative contribution of individual storms. Thirty percent of TS drove mobility at three or four of the mid-shelf sites considered here, indicating their spatial influence away from the storm wind field. The wave stress caused by ETS was primarily confined to areas within the storm wind field. However, the broad wind fields associated with these storms resulted in mobility events caused by winds from low-pressure centers over the Gulf of Mexico, the central U.S., and offshore.

In the MAB, frequent ETS resulted in a dominant impact of these storms, accounting for 61–68% of mobility hours and 67–87% of IWAVES. In the SAB, 34–41% of mobility hours and 66–67% of IWAVES were driven by relatively infrequent but powerful TS. These TS were located to the south and southeast of the SAB, and produced waves that generated stress events as far north as Cape Cod. Over the period of 1990–2012, sediment mobility was estimated to occur more frequently at mid-shelf depths in the MAB than in the SAB, likely due to the combined impact in the MAB of far-field TS and near-field ETS. Northward propagating waves generated in the strong northeast quadrant of storms and the eastward protrusion of Cape Hatteras resulted in little or no mobility in the SAB driven by storms located offshore of Cape Hatteras and points north.

Acknowledgments

The authors thank Joseph Long and three anonymous peer

reviewers for their evaluations. This work was funded by the U.S. Geological Survey.

References

Airy, G.B., 1845. Tides and waves, Section 392. Encycopedia Metropolitana, vol. 5; 1845, pp. 241–396.

Ardhuin, F., Drake, T.G., Herbers, T.H.C., 2002. Observations of wave-generated vortex ripples on the North Carolina continental shelf. J. Geophys. Res. 107 (C10). http://dx.doi.org/10.1029/2001jc000986 7-1.

Ardhuin, F., O'Reilly, W.C., Herbers, T.H.C., Jessen, P.F., 2003. Swell transformation across the continental shelf. Part I: attenuation and directional broadening. J. Phys. Oceanogr. 33 (9), 1921–1939. http://dx.doi.org/10.1175/1520-0485(2003)033<1921:STATCS>2.0.CO;2.

Aucan, J., Ardhuin, F., 2013. Infragravity waves in the deep ocean: an upward revision. Geophys. Res. Lett. 40, 3435–3439. http://dx.doi.org/10.1002/grl.50321.

Austin, J.A., Lentz, S.J., 1999. The relationship between synoptic weather systems and meteorological forcing on the North Carolina inner shelf. J. Geophys. Res. 104 (C8), 18159–18185. http://dx.doi.org/10.1029/1999JC900016.

Bengtsson, L., Hodges, K.I., Roeckner, E., 2006. Storm track and climate change. J. Climate 19 (15), 3518–3543. http://dx.doi.org/10.1175/JCLI3815.1.

Berty, H.P., Shi, H., Lyons-Weiler, J., 2010. Determining the statistical significant of survivorship prediction models. J. Eval. Clin. Pract. 16 (1), 155–165. http://dx.doi.org/10.1111/j.1365-2753.2009.01199.x.

Butman, B., Noble, M., Folger, D.W., 1979. Long-term observations of bottom current and bottom sediment movement on the mid-Atlantic continental shelf. J. Geophys. Res. 84 (C3), 1187–1205. http://dx.doi.org/10.1029/JC084iC03p01187.

Butman, B., Sherwood, C.R., Dalyander, P.S., 2008. Northeast storms ranked by wind stress and wave-generated bottom stress observed in Massachusetts Bay, 1990–2006. Cont. Shelf Res. 28 (10–11), 1231–1245. http://dx.doi.org/10.1016/j.csr.2008.02.010.

Chang, G.C., Dickey, T.D., Williams III, A.J., 2001. Sediment resuspension over a continental shelf during Hurricanes Edouard and Hortense. J. Geophys. Res. 106 (C5), 9517–9531. http://dx.doi.org/10.1029/2000JC900032.

Chawla, A., Cao, D., Gerald, V.M., Spindler, T., Tolman, H.L., 2007. Operational implementation of a multi-grid wave forecast systems. In: Proceedings of the 10th International Workshop on Wave Hindcasting and Forecasting & Coastal Hazard Symposium Paper B3.

Churchill, J.H., Wirick, C.D., Flagg, C.N., Pietrafesa, L.J., 1994. Sediment resuspension over the continental shelf east of the Delmarva Peninsula. Deep Sea Res. Part II: Top. Stud. Oceanogr. 41 (2–3), 341–363. http://dx.doi.org/10.1016/0967-0645(94)90027-2.

Dalyander, P.S., Butman, B., Sherwood, C.R., Signell, R.P., Wilkin, J.W., 2013. Characterizing wave- and current-induced bottom shear stress: U.S. Middle Atlantic Bight. Cont. Shelf Res. 52, 73–86. http://dx.doi.org/10.1016/j.csr.2012.10.012.

Davis, R.E., Dolan, R., Demme, G., 1993. Synoptic climatology of Atlantic coast northeasters. Intl. J. Climatol. 13 (2), 171–189. http://dx.doi.org/10.1002/joc.3370130204.

Dolan, R., Davis, R.E., 1992. An intensity scale for Atlantic coast northeast storms. J. Coastal Res. 8 (4), 352–364.

Drake, D.E., Cacchione, D.A., 1985. Seasonal variation in sediment transport on the Russian River shelf, California. Cont. Shelf Res. 4 (5), 495–514. http://dx.doi.org/10.1016/0278-4343(85)90007-X.

Dufois, F., Garreau, P., Le Hir, P., Forget, P., 2008. Wave- and current-induced bottom shear stress distribution in the Gulf of Lions. Cont. Shelf Res. 28 (15), 1920–1934. http://dx.doi.org/10.1016/j.csr.2008.03.028.

Elfrink, B., Hanes, D.M., Ruessink, G., 2006. Parameterization and simulation of near bed orbital velocities under irregular waves in shallow water. Coast. Eng. 53 (11), 915–927. http://dx.doi.org/10.1016/j.coastaleng.2006.06.002.

Gagan, M.K., Chivas, A.R., Herczeg, A.L., 1990. Shelf-wide erosion, deposition, and suspended sediment transport during Cyclone Winifred, Central Great Barrier Reef, Australia. J. Sed. Pet. 60 (3), 456–470. http://dx.doi.org/10.1306/212F91BF-2B24-11D7-8648000102C1865D.

Ginsburg, R.N., James, N.P., 1974. Holocene carbonate sediments of continental shelves. In: Burk, C.A., Drake, C.L. (Eds.), The Geology of Continental Margins. Springer-Verlag, Berlin, Germany, pp. 137–155. http://dx.doi.org/10.1007/978-3-662-01141-6_11.

Grant, W.D., Madsen, O.S., 1979. Combined wave and current interaction with a rough bottom. J. Geophys. Res.: Oceans 84 (C4), 1797–1808. http://dx.doi.org/10.1029/jc084ic04p01797.

Harris, P.T., Coleman, R., 1998. Estimating global shelf sediment mobility due to swell waves. Mar. Geol. 150 (1–4), 171–177. http://dx.doi.org/10.1016/S0025-3227(98)00040-1.

Hart, R.E., Grumm, R.H., 2001. Using normalized climatological anomalies to rank synoptic-scale events objectively. Mon. Weather Rev. 129 (9), 2426–2442. http://dx.doi.org/10.1175/1520-0493(2001)129<2426:UNCATR>2.0.CO;2.

Hasselmann, 1962. On the non-linear energy transfer in a gravity-wave spectrum, Part 1: general theory. J. Fluid Mech. 12, 481–500. http://dx.doi.org/10.1017/S0022112062000373.

Hasselmann, K., Barnett, T.P., Bouws, E., Carlson, H., Cartwright, D.E., Enke, K., Ewing, J.A., Gienapp, H., Hassellman, D.E., Kruseman, P., Meerburg, A., Müller, P., Olbers, D.J., Richter, K., Sell, W., Walden, H., 1973. Measurements of wind-wave growth and swell decay during the joint North Sea wave project (JONSWAP): Hamburg, Germany. Deut. Hydrogr. Inst. Ergänz. Deut. Hydrogr. Z. Reihe A 8, 95.

Herbers, T.H.C., Elgar, S., Guza, R.T., 1994. Infragravity-frequency (0.005–0.05 Hz) motions on the shelf, Part I, forced waves. J. Phys. Oceanogr. 24 (5), 917–927, doi: 10.1175/1520-0485(1994)024<0917:IFHMOT>2.0.CO;2.

Herbers, T.H.C., Elgar, S., Guza, R.T., O'Reilly, W.C., 1995a. Infragravity-frequency (0.005–0.05 Hz) motions on the shelf, Part II, free waves. J. Phys. Oceanogr 25 (6), 1063–1079, doi:10.1175/1520-0485(1995)025<1063:IFHMOT>2.0.CO;2.

Herbers, T.H.C., Elgar, S., Guza, R.T., 1995b. Generation and propagation of infragravity waves. J. Geophys. Res. 100 (C12), 24863–24872. http://dx.doi.org/10.1029/95JC02680.

Herbers, T.H.C., Hendrickson, E.J., O'Reil, W.C., 2012. Propagation of swell across a wide continental shelf. J. Geophys. Res. 105 (C8), 19729–19737. http://dx.doi.org/10.1029/2000JC900085.

Hurther, D., Thorne, P.D., 2011. Suspension and near-bed load sediment transport processes above a migrating, sand-rippled bed under shoaling waves. J. Geophys. Res.: Oceans 116 (C7), 2156–2202. http://dx.doi.org/10.1029/2010JC006774.

Kaplan, E.L., Meier, P., 1958. Nonparametric estimation from incomplete observations. J. Am. Stat. Assoc. 53 (282), 457–481. http://dx.doi.org/10.1007/springerreference_205495.

Keim, B.D., Muller, R.A., Stone, G.W., 2004. Spatial and temporal variability of coastal storms in the North Atlantic Basin. Mar. Geol. 210 (1–4), 7–15. http://dx.doi.org/10.1016/j.margeo.2003.12.006.

Kohut, J.T., Glenn, S.M., Paduan, J.D., 2006. Inner shelf response to Tropical Storm Floyd. J. Geophys. Res. 111 (C9), C09S91. http://dx.doi.org/10.1029/2003JC002173.

Komar, P.D., 1998. Beach Processes and Sedimentation. Prentice Hall, Inc., Upper Saddle River, New Jersey, USA.

Kim, S.-C., Wright, L.D., Kim, B.-O., 1997. The combined effects of synoptic-scale and local-scale meteorological events on bed stress and sediment transport on the inner shelf of the Middle Atlantic Bight. Cont. Shelf Res. 17 (4), 407–433. http://dx.doi.org/10.1016/S0278-4343(96)00038-6.

Kirtman, B., Power, S.B., Adedoyin, J.A., Boer, G.J., Bojariu, R., Camilloni, I., Doblas-Reyes, F.J., Fiore, A.M., Kimoto, M., Meehl, G.A., Prather, M., Sarr, A., Schär, C., Sutton, R., van Oldenborgh, G.J., Vecchi, G., Wang, H.J., 2013. Near-term Climate Change: Projections and Predictability. In: Stocker, T.F., Qin, D., Plattner, G.-K., Tignor, M., Allen, S.K., Boschung, J., Nauels, A., Xia, Y., Bex, V., Midgley, P.M. (Eds.), Climate Change 2013: The Physical Science Basis. Contribution of Working Group I to the Fifth Assessment Report of the Intergovernmental Panel on Climate Change. Cambridge University Press, Cambridge, United Kingdom and New York, NY, USA.

Lawrence, M.B., Avila, L.A., Beven, J.L., Franklin, J.L., Guiney, J.L., Pasch, R.J., 2001. Atlantic Hurricane Season of 1999. Mon. Weather Rev. 129, 3057–3084. http://dx.doi.org/10.1175/1520-0493(2001)129<3057:AHSO>2.0.CO;2.

Li, M.Z., 1994. Direct skin friction measurements and stress partitioning over movable sand ripples. J. Geophys. Res. 99 (C1), 791–799. http://dx.doi.org/10.1029/93JC02445.

Longuet-Higgins, M.S., Stewart, R.W., 1962. Radiation stress and mass transport in gravity waves, with application to 'surf beats. J. Fluid Mech. 13 (4), 481–504. http://dx.doi.org/10.1017/S0022112062000877.

Longuet-Higgins, M.S., Stewart, R.W., 1964. Radiation stresses in water waves; a physical discussion, with applications. Deep Sea Res. 11 (4), 529–562. http://dx.doi.org/10.1016/0011-7471(64)90001-4.

Lyne, V.D., Butman, B., Grant, W.D., 1990a. Sediment movement along the U.S. east coast continental shelf—I. Estimates of bottom stress using the Grant-Madsen model and near-bottom wave and current measurements. Cont. Shelf Res. 10 (5), 397–428, doi: 10.1016/0278-4343(90)90048-Q.

Lyne, V.D., Butman, B., Grant, W.D., 1990b. Sediment movement along the U.S. east coast continental shelf—II. Modelling suspended sediment concentration and transport rate during storms. Cont. Shelf Res. 10 (5), 429–460. http://dx.doi.org/10.1016/0278-4343(90)90049-R.

Madsen, O.S., 1994. Spectral wave-current bottom boundary layer flows. In: Proceedings of the 24th Conference on Coastal Engineering. pp. 384–398.

Mantel, N., 1966. Evaluation of survival data and two new rank order statistics arising in its consideration. Cancer Chemother. Rep. Part 1 50 (3), 163–170.

Mather, J.R., Adams III, H., Yoshioka, G.A., 1964. Coastal storms of the eastern United States. J. Appl. Meteor. 3 (6), 693–706. http://dx.doi.org/10.1175/1520-0450(1964)003<0693:CSOTEU>2.0.CO;2.

McAdie, C.J., Landsea, C.W., Neumann, C.J., David, J.E., Blake, E.S., Hammer, G.R., 2009. Tropical Cyclones of the North Atlantic Ocean, 1851–2006. National Oceanic and Atmospheric Administration Historical Climatology Series 6-2.

McMullen, K.Y., Paskevich, V.F., Poppe, L.J., 2011. GIS data catalog (version 2.2). In: Poppe, L.J., Williams, S.J., Paskevich, V.F. (Eds.), 2005, USGS East-Coast Sediment Analysis: Procedures, Database, and GIS Data, U.S. Geological Survey Open-File Report 2005-1001. Available online at: ⟨http://woodshole.er.usgs.gov/openfile/of2005-1001/htmldocs/datacatalog.htm⟩.

Miles, T., Glenn, S.M., Schofield, O., 2013. Temporal and spatial variability in fall storm induced sediment resuspension on the Mid-Atlantic Bight. Cont. Shelf Res. 63 (Suppl.), S36–S49. http://dx.doi.org/10.1016/j.csr.2012.08.006.

Munk, W.H., 1949. Surf beats. EOS Trans. AGU Trans. 30 (6), 849–854.

National Hurricane Center, Hurricane Research Division, 2014. Atlantic hurricane best track (HURDAT version 2). United States National Oceanic and Atmospheric Administration. Online at: ⟨http://www.aoml.noaa.gov/hrd/hurdat/Data_Storm.html⟩ (accessed12.12.13).

Nielsen, P., 1992. Coastal Bottom Boundary Layers and Sediment Transport. World Scientific Publications, Singaporehttp://dx.doi.org/10.1142/9789812796035.

Oberle, F.K.J., Storlazzi, C.D., Hanebuth, T.J.J., 2014. Wave-driven sediment mobilization on a storm-controlled continental shelf (Northwest Iberia). J. Mar. Syst. 139, 362–372. http://dx.doi.org/10.1016/j.jmarsys.2014.07.018.

Porter-Smith, R., Harris, P.T., Andersen, O.B., Coleman, R., Greenslade, D., Jenkins, C. J., 2004. Classification of the Australian continental shelf based on predicted sediment threshold exceedance from tidal currents and swell waves. Mar. Geol. 211 (1–2), 1–20. http://dx.doi.org/10.1016/j.margeo.2004.05.031.

Rankin, K.L., Hires, R.I., 2000. Laboratory measurement of bottom shear stress on a movable bed. J. Geophys. Res. 105 (C7), 17,011–17,019. http://dx.doi.org/10.1029/2000JC900059.

Reid, J.M., Reid, J.A., Jenkins, C.J., Hastings, M.E., Williams, S.J., Poppe, L.J., 2005. usSEABED: Atlantic coast Offshore Surficial Sediment Data Release. U.S. Geological Survey Data Series 118, version 1.0. Available online at: ⟨http://pubs.usgs.gov/ds/2005/118⟩.

Ruessink, B.G., 1998. Bound and free infragravity waves in the nearshore zone under breaking and nonbreaking conditions. J. Geophys. Res. 103 (C6), 12,795–12,805. http://dx.doi.org/10.1029/98JC00893.

Saha, S., Moorthi, S., Pan, H.-L., Wu, X., Wang, J., Nadiga, S., Tripp, P., Kistler, R., Woollen, J., Behringer, D., Liu, H., Stokes, D., Grumbine, R., Gayno, G., Wang, J., Hou, Y.-T., Chuang, H.-Y., Juang, H.-M.H., sela, J., Iredell, M., Treadon, R., Kleist, D., Van Delst, P., Keyser, D., Derber, J., Ek, M., Meng, J., Wei, H., Yang, R., Lord, S., van den Dool, H., Kumar, A., Wang, W., Long, C., chelliah, M., Xue, Y., Huang, B., Schemm, J.-K., Ebisuzaki, W., Lin, R., Xie, P., Chen, M., Zhoi, S., Higgins, W., Zou, C.-Z., Liu, Q., Chen, Y., Han, Y., Cucurull, L., Reynolds, R.W., Rutledge, G., Goldberg, M., 2010. The NCEP climate forecast system reanalysis. Am. Meteorol. Soc. 91 (8), 1015–1057. http://dx.doi.org/10.1175/2010BAMS3001.1.

Serreze, M.C., 2009. Northern Hemisphere Cyclone Locations and Characteristics from NCEP/NCAR Reanalysis Data. Boulder, Colorado USA: National Snow and Ice Data Center. Online at: ⟨https://nsidc.org/data/docs/daac/nsidc0423_cyclone/⟩ (accessed 10.01.14).

Sherwood, C.R., Butman, B., Cacchione, D.A., Drake, D.E., Gross, T.F., Sternberg, R.W., Wibert, P.L., Williams III, A.J., 1994. Sediment-transport events on the northern California continental shelf during the 1990–1991 STRESS experiment. Cont. Shelf Res. 14 (10), 1063–1099. http://dx.doi.org/10.1016/0278-4343(94)90029-9.

Shields, A., 1936. Anwendung der Aehnlichkeitsmechanik und der Turbulenzforschung auf die Geschiebebewegung [Application of similarity mechanics and turbulence research on shear flow], Mitteilungen der Preußischen Versuchsanstalt für Wasserbau (in German) 26. Preußische Versuchsanstalt für Wasserbau, Berlin.

Simpson, R.H., 1974. The hurricane disaster potential scale. Weatherwise 27 (8), 169. http://dx.doi.org/10.1080/00431672.1974.9931702.

Simpson, R.H., Riehl, H., 1981. The Hurricane and Its Impact. Louisiana State University Press, Baton Rouge, Louisiana, USA.

Smaoui, H., Ouahsine, A., 2012. Extension of the skin shear stress Li's relationship to the flat bed. Env. Fluid Mech. 12 (3), 201–207. http://dx.doi.org/10.1007/s10652-011-9231-2.

Snedden, J.W., Nummedal, D., Amos, A.F., 1988. Storm and fair weather combined flow on the central Texas continental shelf. J. Sed. Res. 58 (4), 580–595, doi: 212F8DFA-2B24-11D7-8648000102C1865D.

Soulsby, R., 1997. Dynamics of Marine Sands, a Manual for Practical Applications. Thomas Telford Publications, London, UKhttp://dx.doi.org/10.1680/doms.25844.

Symonds, G., Huntley, D.A., Bowen, A.J., 1982. Two-dimensional surf beat: Long wave generation by a time-varying breakpoint. J. Geophys. Res. 87 (C1), 492–498. http://dx.doi.org/10.1029/jc087ic01p00492.

Tolman, H.L., 2007. Development of a Multi-grid Version of WAVEWATCH III. Technical Note 256, NCEP/NOAA/NWS. National Center for Environmental Prediction, Washington, D.C.

Tolman, H.L., 2009. User manual and system documentation of WAVEWATCH III version 3.14. Technical Note 276. NCEP/NOAA/NWS. National Center for Environmental Prediction, Washington, D.C.

Tucker, M.J., 1950. Surfbeats: Sea waves of 1 to 5 minutes period. Proc. R. Soc. London, Ser. A 202, 565–573. http://dx.doi.org/10.1098/rspa.1950.0120.

Twichell, D.C., McClennen, C.E., Butman, B., 1981. Morphology and processes associated with the accumulation of the fine-grained sediment deposit on the southern New England shelf. J. Sed. Res. 51 (1), 269–280. http://dx.doi.org/10.1306/212F7C6B-2B24-11D7-8648000102C1865D.

Warner, J.C., Armstrong, B., Sylvester, C.S., Voulgaris, G., Nelson, T., Schwab, W.C., Denny, J.F., 2012. Storm-induced inner-continental shelf circulation and sediment transport: Long Bay, South Carolina. Cont. Shelf Res. 42, 51–63. http://dx.doi.org/10.1016/j.csr.2012.05.001.

Wiberg, P.L., Sherwood, C.R., 2008. Calculating wave-generated bottom orbital velocities from surface wave parameters. Comp. Geosci. 34 (10), 1243–1262. http://dx.doi.org/10.1016/j.cageo.2008.02.010.

Zhang, K., Douglas, B.C., Leatherman, S.P., 2000. Twentieth-century storm activity along the U.S. East Coast. J. Clim. 13 (10), 1748–1761. http://dx.doi.org/10.1175/1520-0442(2000)013 < 1748:TCSAAT > 2.0.CO;2.

Zhang, K., Douglas, B.C., Leatherman, S.P., 2001. Beach erosion potential for severe Nor'Easters. J. Coast. Res. 17 (2), 309–321.

Zielinski, G.A., 2002. A classification scheme for winter storms in the eastern and central United States with an emphasis on nor'easters. Bull. Am. Meteorol. Soc. 83 (1), 37–51. http://dx.doi.org/10.1175/1520-0477(2002)083 < 0037:ACSFWS > 2.3.CO;2.